Geothermics, Vol. 17, No. 5/6, pp. 695–710, 1988.
Printed in Great Britain.

0375–6505/88 $3.00 + 0.00
Pergamon Press plc

EVOLUTION OF THE THERMAL CAP IN TWO WELLS FROM THE SALTON SEA GEOTHERMAL SYSTEM, CALIFORNIA

JOSEPH N. MOORE and MICHAEL C. ADAMS

University of Utah Research Institute, 391 Chipeta Way, Suite C, Salt Lake City, UT 84108-1295, U.S.A.

(*Received January* 1988; *accepted for publication April* 1988)

Abstract—The Salton Sea geothermal system is located near the center of the sediment-filled Salton Trough where temperatures locally reach 365°C at depths of 2 km. The geothermal reservoir is overlain by a thermal cap of low-permeability rocks that restricts the upward movement of the high-temperature brines. Petrographic and fluid-inclusion studies in two wells drilled in the southern part of the field indicate that the thermal cap consists of an upper layer of lacustrine and evaporite deposits with low initial permeabilities and a lower layer of deltaic sandstones. The sandstones were incorporated into the thermal cap as downward percolating fluids deposited anhydrite and calcite in the pore space of the rocks, reducing their permeabilities. During development of the thermal cap, base-metal sulfides, potassium feldspar and quartz were deposited by brines from higher-temperature portions of the system.

INTRODUCTION

The Salton Sea geothermal system of southern California is among the largest of the thermal centers occurring in the sediment-filled Salton Trough (Fig. 1). Mineral assemblages and textures formed in response to geothermal activity at the Salton Sea can be categorized as diagenetic or metamorphic (McKibben and Elders, 1985). Diagenetic processes occur at temperatures of less than about 250°C and have resulted in the recrystallization of the sheet silicates and the deposition of anhydrite, carbonates and sulfides in the pore space of the sediments (McDowell and Paces, 1985; McKibben and Elders, 1985). The reduction in the permeabilities of the shallow sediments caused by the deposition of these pore-filling minerals has led to the development of a thick thermal cap, or zone of conductive heating, over the reservoir (Younker *et al.*, 1982). As shown by Younker *et al.* (1982), the thermal cap in general does not correspond to the lithologic caprock of Randall (1974) or the carbonate cap described by McDowell and Elders (1979) and McDowell and Paces (1985). Metamorphic processes occurring in the reservoir, where temperatures range from 250 to 365°C, have led to the development of hornfelsic textures and mineral assemblages typical of the greenschist facies (Muffler and White, 1969; McDowell and Elders, 1979). Fluids encountered at the depths where these metamorphic processes are occurring have salinities of up to 25 weight % (Helgeson, 1968).

In contrast to the deep portions of the Salton Sea geothermal system, where fluids are sampled directly from the production wells, few data have been presented on the temperatures and salinities of the brines that have characterized the upper parts of the geothermal field. Furthermore, because there is evidence that conditions within the geothermal system have changed with time (Skinner *et al.*, 1967; Huang, 1977; Andes and McKibben, 1987), the present borehole temperatures and fluids may not accurately reflect the conditions associated with the alteration of the shallow sediments. Alternatively, these data can be obtained from micro-

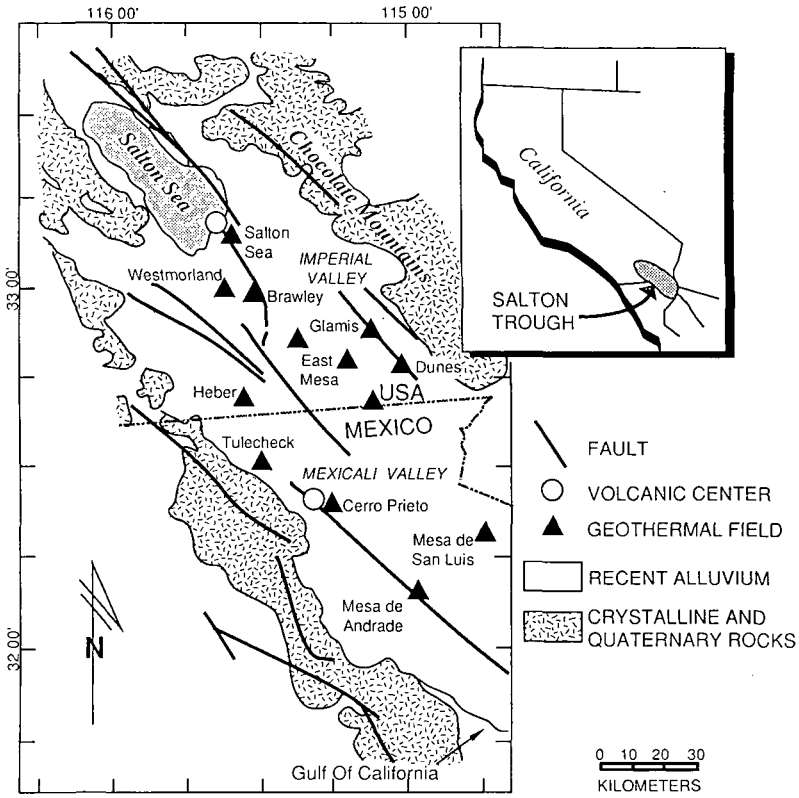

Fig. 1. Distribution of geothermal fields in the Salton Trough. Modified from Elders and Cohen (1983).

thermometric measurements of fluid inclusions contained within the authigenic minerals. In this paper we describe the results of fluid inclusion and petrographic studies of two boreholes which contain abundant shallow anhydrite, sphalerite and vein quartz suitable for microthermometric studies. The data are used to describe the evolution of the thermal cap penetrated in these wells and the prominent sphalerite mineralization they contain. The samples studied were provided by UNOCAL from two boreholes drilled in the southern part of the field (Fig. 2). Temperature–depth data from these wells have not yet been released into the public domain.

LITHOLOGIC AND MINERALOGIC RELATIONSHIPS

The Salton Trough is filled with a thick sequence of sediments that form the Colorado River delta. Within the Salton Sea geothermal system, the sediments can be divided into two sequences (Randall, 1974). The upper sequence consists of lacustrine claystone and evaporite deposits formed in the basin now partially occupied by the Salton Sea. According to Randall (1974), the lacustrine deposits have low initial permeabilities and range in thickness from about 250 m in the southern part of the field to 750 m in the northern part. The lower sequence consists of deltaic sandstones, siltstones and shales that are thought to be no older than Pliocene to Pleistocene in age (Muffler and Doe, 1968).

The two wells described in this paper were sampled to depths of 1646 and 1292 m (wells A and B respectively). Figure 3 details the lithologies and mineral assemblages found in the upper parts of the wells, which have been the focus of our study. These lithologic columns are based on an

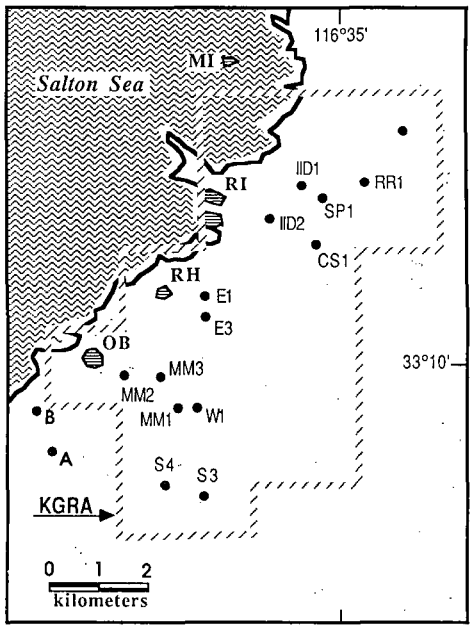

Fig. 2. Well locations in the Salton Sea geothermal field. Wells: CS = California State; E = Elmore; MM = Magmamax; S = Sinclair; SP = Sportsman; W = Woolsey. A and B are the locations of the wells described in this study. Rhyolite domes: MI = Mullet Island; OB = Obsidian Butte; RH = Rock Hill; RI = Rock Island. The hachured line shows the boundary of the original Salton Sea Known Geothermal Resource Area (KGRA). Modified from McDowell and Elders (1980).

examination of drill-chip samples collected at 6 or 9 m (20 or 30 ft) intervals. At greater depths, where the rocks typically contain epidote, recrystallization and the development of metamorphic assemblages have obliterated many diagenetic features.

The lacustrine deposits are 241–277 m thick in these wells. The upper portion of the deposit consists of poorly consolidated, clay-rich sediments, which extend from the surface to a depth of about 140 m. The lower portion of the lacustrine section is composed of interbedded claystone and evaporite deposits.

The primary and secondary minerals we observed in these wells (Fig. 3) are similar to those found in other parts of the field (see for example Muffler and White, 1969; McDowell and Elders, 1979, 1980, 1983). With increasing depth, the secondary assemblages in the rocks we have studied define three zones:

(1) *Interlayered illite/smectite zone.* (0–222 m in well A; 0–241 m in well B) Anhydrite, calcite, interlayered illite/smectite and interlayered chlorite/smectite.

(2) *Chlorite–calcite zone.* (222–616 m in well A; 241–789 m in well B) Chlorite, illite, interlayered chlorite/smectite, calcite, anhydrite, potassium feldspar, quartz, sphene and base-metal sulfides.

(3) *Chlorite–epidote–calcite zone.* (616–1646 m in well A; 789–1292 m in well B) Epidote, calcite, chlorite, quartz, potassium feldspar, albitic plagioclase, anhydrite, illite and sphene.

Traces of pyrite and hematite occur throughout these zones. In the following section, only relationships that are important to understanding the diagenetic history of the rocks shallower than the chlorite–epidote–calcite zone are discussed in detail. The reader is referred to the studies cited above for additional descriptions of the secondary mineral assemblages and textures typical of the Salton Sea geothermal system.

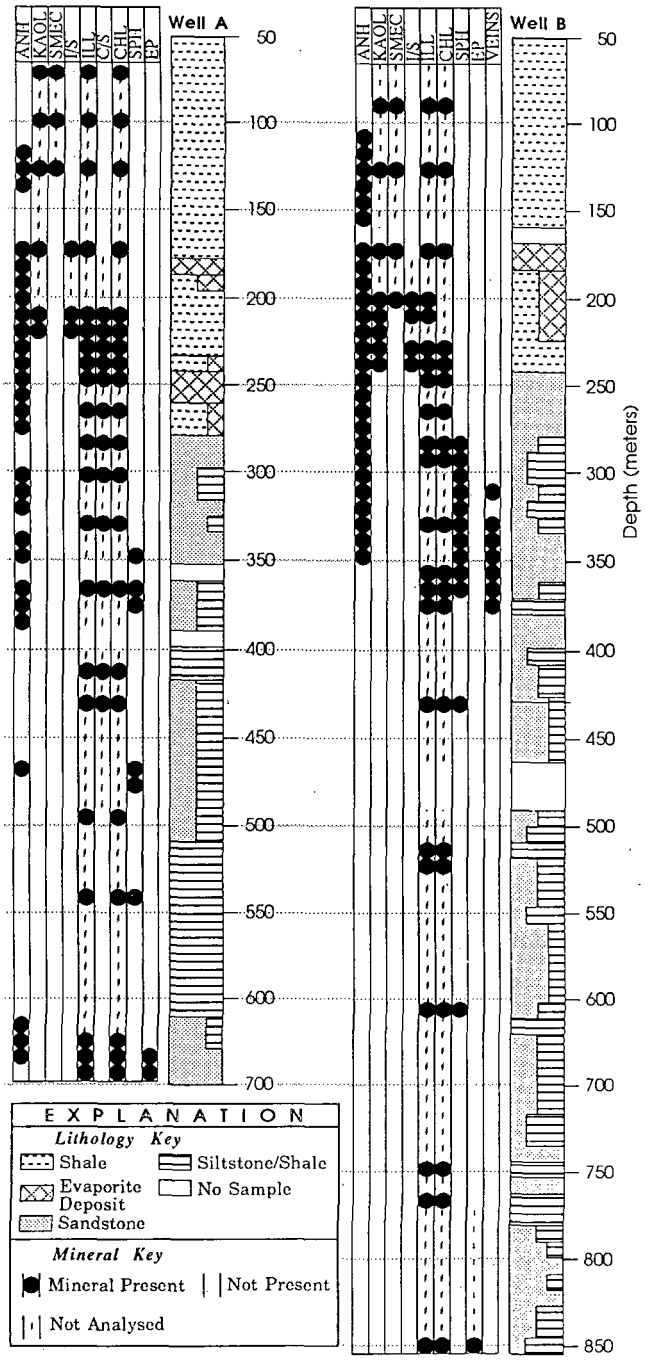

Fig. 3. Lithologies and mineral distributions in the interlayered illite/smectite and chlorite–calcite zones of the two wells studied. Abbreviations: anh = anhydrite, kaol = kaolinite, smec = smectite, I/S = interlayered illite/smectite, ill = illite, I/C = interlayered chlorite/smectite, chl = chlorite, sph = spalerite.

Interlayered illite/smectite zone

The weakly altered rocks of the interlayered illite/smectite zone are distinguished from rocks of the underlying higher-temperature zone by the presence of detrital smectite containing 10–15% randomly interlayered illite, and kaolinite. X-ray analyses of the <5 μm fraction of these rocks indicates that the lower part of this zone is characterized by interlayered illite/smectite (ordered) and chlorite/smectite. The absence of these interlayered minerals from the shallowest samples and their restricted occurrence suggests that they are authigenic in origin. Using relationships presented by Srodon and Eberl (1984), our X-ray analyses indicate that the smectite content of the interlayered illite/smectite decreases from approximately 30–40% in the shallowest samples to 5–20% in samples from the base of this zone.

Both ordered and randomly interlayered varieties of chlorite/smectite are present. The ordered phase has X-ray characteristics corresponding to corrensite. However, because of the presence of overlapping peaks on the X-ray diffraction patterns and the small amount of clay in some samples, it was not possible to determine accurately the distribution of individual interlayered chlorite/smectite minerals in these samples.

Anhydrite occurs throughout the lacustrine deposits as tabular crystals and rosettes in the claystones and as aggregates associated with carbonate in the evaporite beds. Muffler and Doe (1968) concluded that the anhydrite in these rocks formed by the dehydration of gypsum, which is common in deposits on the margins of the Salton Trough. Fine-grained gypsum was identified optically and confirmed by X-ray analysis in samples from the wells we studied. However, the textural relationships suggest that the gypsum represents an alteration product of anhydrite and is not a primary phase in these rocks.

Chlorite–calcite zone

The transition from the weakly altered rocks in the upper part of the wells to the chlorite–calcite zone is marked by the transformation of interlayered illite/smectite to illite and the formation of significant chlorite. The results of the X-ray analyses shown in Fig. 3 suggest that chlorite may have formed by several different reactions. The lack of kaolinite in samples below 241 m in well B and the increase in chlorite at this depth suggest that chlorite initially formed from reactions involving kaolinite and carbonates, as proposed by Muffler and White (1969). However, our X-ray data suggest that the amount of kaolinite present cannot account for the abundance of chlorite in this well. Thus, in well B, reactions involving detrital smectite may also have been important (McDowell, written comments, 1987).

The absence of kaolinite below 223 m in well A, and the presence of only traces of smectite below this depth suggest that at least some of the chlorite has formed from these detrital minerals. In addition, the X-ray data suggest that chlorite has formed from reactions involving interlayered chlorite/smectite, which is the major component of the clay fraction between 232 and 369 m. With increasing depth, the smectite content of the interlayered chlorite/smectite decreases from approximately 40–50% between 204 and 287 m to approximately 10% at 360 m. We conclude from these relationships that detrital chlorite was altered to interlayered chlorite/smectite which then reacted with the brines to form secondary chlorite.

The sandstones of the chlorite–calcite zone are cemented by variable proportions of anhydrite, calcite, chlorite, quartz, base-metal sulfides and potassium feldspar. Anhydrite and calcite are the dominant pore-filling minerals in the non-argillaceous sandstones from depths shallower than 387 m in well A and 351 m in well B. Although a few narrow intervals of anhydrite-rich rocks occur below 450 m in well A (457–466 m, 610–628 m), the abundance and coarse grain size of the anhydrite suggests that it was derived from thin evaporite deposits interbedded with the deltaic sediments.

Sphalerite is the most abundant of the pore-filling sulfide minerals, occurring in amounts of up to several % in the anhydrite-bearing sandstones (Fig. 3). In many samples, minor amounts of galena and chalcopyrite are also present as a replacement of sphalerite. In thin-section the sphalerite is typically seen as anhedral grains that contain inclusions of anhydrite as well as numerous inclusions of detrital quartz and feldspar. These lithologic and petrographic relationships indicate that base-metal deposition occurred after the initial permeabilities of the sandstones had been reduced by anhydrite and calcite cement. Similar zones of shallow base-metal mineralization have been observed by McKibben and Elders (1985, Fig. 6f) at 404 m in Magmamax No. 2 and at 450 m in River Ranch No. 1.

Pore-filling potassium feldspar and quartz are found in both wells below a depth of 300 m. In addition to occurring as overgrowths on grains of detrital feldspar, secondary potassium feldspar is found as a replacement of detrital plagioclase between depths of 300 and 600 m. As discussed in detail below, the occurrence of secondary potassium feldspar and quartz throughout this zone provides strong evidence for the influx of brines from deeper parts of the geothermal system.

Quartz veins containing minor barite, chlorite, hematite, and traces of galena, sphalerite, calcite and anhydrite occur between depths of 305 and 378 m in well B (Fig. 3). Barite is an uncommon mineral in the Salton Sea geothermal system. In these veins, it is found as embayed crystals surrounded by quartz. In contrast, galena typically occurs as euhedral crystals that clearly postdate quartz in places. From these textural relationships we infer that barite was deposited early and the sulfide minerals late in the vein paragenesis.

Chlorite–epidote–calcite zone

The highest-grade assemblages found in the two wells studied are characterized by the occurrence of epidote. Epidote occurs as small prismatic crystals in the matrix of the sandstones at depths greater than 616 m in well A and 789 m in well B (refer to Fig. 3). In contrast to samples from shallower depths, both potassium feldspar and plagioclase appear to be stable secondary phases within this zone.

FLUID-INCLUSION DATA

Fluid inclusions in anhydrite, sphalerite and vein quartz were studied (Table 1). The petrographic data described above suggest that the deposition of anhydrite began prior to both sphalerite cementation and quartz veining. Thus, primary and secondary fluid inclusions in anhydrite can potentially provide information on the temperatures and compositions of the brines that have circulated through the upper portions of the geothermal system since its early evolution. In contrast, inclusions in vein quartz provide information associated with the episodic upwelling of brines from deeper parts of the system. Most of the fluid-inclusion data from the Salton Sea geothermal system are of this latter type (Skinner *et al.*, 1967; Huang, 1977; Freckman, 1978; Andes and McKibben, 1987; Roedder and Howard, 1987). As discussed below, the deposition of sphalerite cement in the sandstones must have occurred prior to quartz veining.

All the fluid inclusions examined in this study were liquid-rich and contained a small vapor bubble that occupied about 20% of the inclusion volume at room temperature. No evidence of a separate gas phase was observed in these inclusions, and with the exception of anhydrite from 168–177 m in well B, none of the inclusions found contained any solid phases.

Fluid-inclusion heating and freezing measurements were made using a Fluid Inc. heating/freezing system. All measurements were made in duplicate. Replicate measurements were within $\pm 0.2°C$. Most of the inclusions studied had maximum dimensions in the range of 2–10 μm.

Table 1. Range of homogenization (T_h°C) and ice-melting (T_m°C) temperatures of fluid inclusions in anhydrite, sphalerite and quartz

Well and depth (m)	Mineral	T_h°C	T_m°C	Type*
A: 177–186	Anhydrite	163–170 (5)†	−6.5 to −7.3 (4)	U
A: 222–232	Anhydrite	168–170 (3)	−4.7 (2)	U
A: 277–287	Anhydrite	228 (6)		U
A: 296–305	Anhydrite	216–235 (12)	−6.7 to −15.3 (10)	S
A: 305–314	Anhydrite	237–239 (5)	−7.9 to −8.0 (2)	S
A: 314–323	Anhydrite	236–241 (9)	−7.3 to −12.8 (11)	S
A: 369–378	Anhydrite	244–245 (3)	−11.7 (1)	S
A: 460–469	Anhydrite	276–282 (5)	−12.9 to −17.5 (5)	U
A: 604–610	Anhydrite	272–288 (10)	−11.7 to −17.1 (21)	U
A: 616–622	Anhydrite	280–284 (3)	−15.1 to −17.7 (6)	S
	Anhydrite	280–282 (4)	−13.8 to −17.5 (19)	U
B: 168–177	Anhydrite	123–129 (11)	−18.5 to −21.4 (9)	P
B: 259–268	Anhydrite	202–213 (13)	−8.4 to −9.2 (4)	S
	Anhydrite	204–221 (6)	−7.7 to −9.8 (5)	U
B: 277–287	Anhydrite	217–218 (4)	−11.2 to −15.2 (3)	S
	Anhydrite	214–227 (10)	−10.5 to −11.3 (7)	U
B: 287–296	Anhydrite	221–236 (11)	−10.8 to −14.5 (12)	U
B: 305–314	Anhydrite	227–233 (5)	−11.0 to −11.5 (2)	S
	Quartz	194–226 (10)	−9.2 to −9.8 (5)	P
	Quartz	182–215 (12)	−0.7 to −6.6 (8)	S
	Sphalerite	179–216 (12)	−10.0 to −10.1 (5)	P
B: 323–332	Anhydrite	239–249 (2)	−15.2 (1)	U
	Quartz	215–242 (29)	−10.5 to −13.9 (7)	P
B: 332–341	Anhydrite	244 (1)		S
	Anhydrite	243–249 (7)	−11.5 to −12.8 (6)	U
B: 341–351	Quartz	215–233 (13)	−11.0 to −12.2 (5)	P
	Quartz	189–198 (5)	−15.2 to −16.5	S
	Sphalerite	209–223 (7)	−10.8 to −12.0 (7)	P

* Type of inclusion: P = primary; S = secondary or pseudosecondary; U = undefined.
† Number of inclusions studied.

In order to assure the validity of our data, fluid inclusions in anhydrite from three depth intervals were systematically overheated to determine their stretching characteristics.

Inclusions in anhydrite

Most of the anhydrite in the drill-chip samples occurs as aggregates of small crystals or as cleavage fragments up to 2 mm across. Because of the difficulties involved in preparing good polished sections from this material, the larger cleavage flakes were studied whenever possible. Primary inclusions were observed only in samples from 168–177 m in well B. These inclusions form three-dimensional arrays that define growth zones in the cleavage fragments. The primary inclusions contain a small ($<1\,\mu$m), unidentified birefringent daughter mineral. In most samples, several generations of fluid inclusions are present. These inclusions occur as trains of secondary or pseudosecondary inclusions occurring along healed fractures or as large, flat inclusions that range up to 4 by 40 μm in size. It was generally not possible to classify these larger inclusions as primary, secondary, or pseudosecondary using the criteria discussed by Roedder (1979).

The homogenization temperatures of fluid inclusions in anhydrite from both wells are plotted against depth in Fig. 4a. The data show that irrespective of the origin of the inclusions in these samples, homogenization temperatures vary little within each depth interval, and that the two wells record similar thermal profiles. No pressure correction has been applied to these data because of the shallow depths.

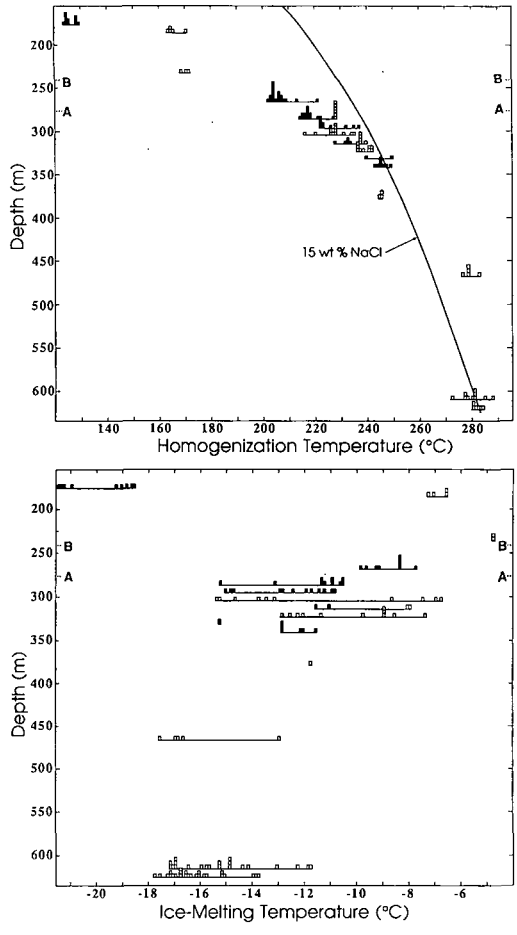

Fig. 4. (a) Homogenization temperature vs depth of fluid inclusions in anhydrite. Symbols: open squares, well A; filled squares, well B. The baselines of the histograms are located at the lowermost limit of the sample interval. Tick marks labeled A and B indicate the depth to the base of the lacustrine deposits in the two wells. The boiling point curve for a 15 weight % NaCl solution (Haas, 1971) is also shown for reference. (b) Ice-melting temperature vs depth for fluid inclusions in anhydrite. Symbols as in Fig. 4a.

Ice-melting temperatures of fluid inclusions in anhydrite (Fig. 4b) range from −21.4 to −4.7°C. Liquid was observed in some of the larger inclusions at temperatures near −50°C (first melting), indicating that the inclusion fluids are enriched in $CaCl_2$, as are the modern brines (Helgeson, 1968). Unfortunately, the small size of the inclusions did not permit an accurate determination of the low-temperature melting relationships in our samples. For reference, freezing-point depressions ranging from 4.7 to 20.8°C correspond to salinities of 7.4 to 23.2 equivalent weight % NaCl according to the equation of Potter *et al.* (1978). This equation is not valid for freezing-point depressions greater than 20.8°C.

It is apparent from an examination of the individual histograms shown in Fig. 4b that there is a wide range of salinities within each depth interval. Despite these compositional variations, differences in the freezing-point depressions of inclusions within texturally distinct groups are small. Frequently, variations within individual groups can be related to refilling of early inclusions by later fluids.

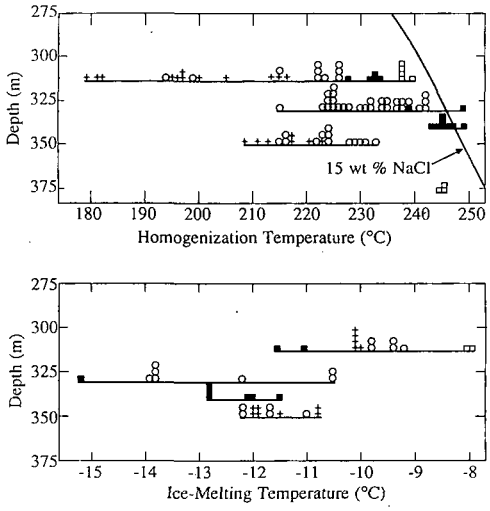

Fig. 5. (a) Homogenization temperature vs depth for fluid inclusions in quartz (circles) and sphalerite (crosses). The boiling point curve and data for anhydrite (open squares, well A; filled squares, well B) from Fig. 4a are shown for reference. (b) Ice-melting temperature vs depth for fluid inclusions shown in Fig. 5a. Symbols as in Fig. 5a.

Inclusions in sphalerite

Fluid inclusions in sphalerite suitable for freezing and heating measurements were found in a few crystals from two depth intervals in well B. The inclusions are primary, forming small isolated groups or three-dimensional arrays that parallel color banding. These inclusions yielded homogenization temperatures ranging from 179 to 223°C (Fig. 5a) and ice-melting temperatures (Fig. 5b) ranging from −12.0 to −10.0°C (16.0–14.0 equivalent weight % NaCl).

Inclusions in quartz

The results of heating and freezing measurements on primary inclusions in euhedral crystals of vein quartz are shown in Figs 5a and 5b. Data were obtained on both primary and secondary inclusions (Table 1). The primary inclusions occur in three-dimensional arrays that define growth zones. Homogenization temperatures of the primary inclusions range from 194 to 242°C. Because of the small size of the inclusions (1–3 μm), only a few freezing-point depressions were measured. The ice-melting temperatures of these inclusions ranged from −13.9 to −9.2°C (17.8–13.1 equivalent weight % NaCl).

Secondary inclusions have homogenization temperatures ranging from 182 to 215°C and ice-melting temperatures that vary from −16.5 to −0.7°C (20.0–1.2 equivalent weight % NaCl). Such a large range of freezing-point depressions requires that the brines had diverse origins. The high-salinity inclusions have freezing-point depressions similar to the brines trapped in anhydrite at these depths and thus may represent locally derived fluids. The low-salinity fluids may represent condensate mixed with a small amount of the higher-salinity brines. No other examples of such low-salinity fluids were found during our study.

Gas analyses of fluid inclusions

Inclusions in ten samples of anhydrite, sphalerite and quartz were selected for gas analysis. The gases were extracted from the inclusions by crushing or laser decrepitation under vacuum and analyzed by mass spectrometry using the techniques described by Sommer (1974) and

Sommer *et al.* (1985). Methane, ethane and propane were detected in addition to carbon dioxide in primary inclusions in sphalerite and quartz. In contrast, inclusions in anhydrite contained mainly carbon dioxide and methane.

Stretching of fluid inclusions in anhydrite

Heating of fluid inclusions, particularly in soft cleavable minerals, can result in an increase in their volume and in their initial or true homogenization temperature (Larson *et al.*, 1973; Bodnar and Bethke, 1984). Bodnar and Bethke (1984) demonstrated that nonelastic increases in volume (stretching) of inclusions in sphalerite and fluorite occurred in a predictable fashion that is related to the properties of the fluid, the size and shape of the inclusions, the temperature they are heated to and the confining pressure. All of the samples they studied required heating above the initial homogenization temperatures to generate internal pressures high enough to cause deformation. In addition, small inclusions required more overheating than large inclusions.

Because of the importance of anhydrite in understanding the evolution of the rocks in the two wells studied and the possibility that anhydrite would be susceptible to stretching, a reconnaissance study of 18 representative inclusions in three cleavage plates was conducted. Inclusions ranging in size from 2 to 40 μm in largest dimension and with bubble diameters between about 0.5 and 2.5 μm (Table 2) were tested. The initial homogenization temperatures and salinities of these inclusions are plotted in Figs 4a and b. The amount of overheating needed to initiate stretching was determined by establishing the initial homogenization temperatures on previously unheated plates and then heating the inclusions in increments of 10°C. All measurements were made in duplicate and were reproducible to within ±0.2°C, even after stretching had increased the homogenization temperature by as much as 50°C. The salinities of these inclusions were determined after heating to avoid the possibility of stretching caused by freezing (Lawler and Crawford, 1983).

Table 2. Change in homogenization temperature (ΔT_h) during overheating (O_h) of inclusions in anhydrite

Sample number	Well	Depth interval (m)	Vapor bubble diameter (mm)*	ΔT_h°C	O_h°C
1	B	259–268	1.5	1.7	31.7 ± 5.0
2	B	259–268	1.0	2.0	51.9 ± 5.0
3	B	259–268	2.0	3.4	35.3 ± 5.0
4	B	259–268	2.0	3.1	23.9 ± 5.0
5	A	277–287	1.0	6.4	15.4 ± 5.0
6	A	277–287	1.0	6.6	45.2 ± 5.0
7	A	277–287	1.8	32.9	55.1 ± 5.0
8	A	277–287	1.5	49.8	45.1 ± 5.0
9	A	277–287	2.3	30.9	35.0 ± 5.0
10	A	277–287	1.0	2.0	45.2 ± 5.0
11	B	332–341	1.0	6.3	35.0 ± 5.0
12	B	332–341	0.8	1.1	53.4 ± 5.0
13	B	332–341	0.5	7.2	52.7 ± 5.0
14	B	332–341	2.0	3.0	9.7 ± 5.0
15	B	332–341	2.5	2.1	20.9 ± 5.0
16	B	332–341	1.5	2.1	5.5 ± 5.5
17	B	332–341	2.5	1.2	33.0 ± 5.0
18	B	332–341	1.0	1.4	62.9 ± 5.0

*The average of the long and short dimensions are given as the diameter for elliptically shaped bubbles.

Table 2 shows that the amount of overheating required to increase the initial homogenization temperature by at least 1°C for all the inclusions tested ranged from 5.5 ± 5.5°C to 55.1 ± 5.0°C and averaged 36.5 ± 5.0°C. Of the 18 inclusions studied however, only three stretched with less than 20°C of overheating. Since none of the intervals in the two wells studied displayed a temperature range greater than 20°C and the plates were not heated above the highest homogenization temperature found during the initial measurements, stretching caused by laboratory heating is not likely to have affected the results reported in this study.

It was not possible to establish accurately the relationship between stretching behavior and inclusion volume because most of the inclusions were flat and many contained small elliptically shaped bubbles. Despite this difficulty, it is apparent from the data in Table 2 that the average amount of overheating needed to initiate stretching was lowest for the large inclusions (average bubble diameter ≥ 2 μm) in each of the depth intervals sampled. The large change in the homogenization temperatures on heating inclusions 7, 8 and 9 (refer to Table 2 for sample numbers) and the small degree of overheating required to increase the homogenization temperature of inclusions 14 and 16 may be the result of leakage.

DISCUSSION

Based on the mineralogic and fluid-inclusion data presented in the preceding sections, the thermal and chemical evolution of the rocks in the low- to moderate-temperature portions of the two wells studied can be established. As discussed in detail below, four distinct processes were involved in the alteration of these rocks. These include: (1) the formation of secondary mineral assemblages through low- to moderate-temperature isochemical reactions; (2) the progressive downward cementation of the lacustrine deposits and shallow deltaic sandstones by anhydrite and calcite; (3) the influx of metal-bearing brines into the upper portion of the deltaic sediments leading to the deposition of sphalerite, potassium feldspar and quartz cement; (4) the development of shallow fracture permeability and the formation of quartz veins.

Diagenetic assemblages and textures produced during heating of the geothermal system are preserved in the rocks encountered above the first appearance of epidote. The distribution of mineral assemblages shown in Fig. 3 support the earlier observations of Muffler and White (1969) and suggest that with increasing temperature, anhydrite was produced from gypsum, illite formed from interlayered illite/smectite and chlorite formed from reactions involving kaolinite, smectite and interlayered chlorite/smectite. Assuming that the fluid inclusions in anhydrite have recorded the maximum temperatures experienced by these rocks because of its retrograde solubility (see below), and that no alteration of the secondary chlorite has occurred since its formation, then the fluid-inclusion data can be used to define the temperature range of the chlorite–calcite zone in these wells. For example, the top of the chlorite–calcite zone occurs at a depth of 241 m in well B. Interpolation of the fluid-inclusion data shown in Fig. 4a indicates that the temperature at this depth would have been approximately 195°C. In a similar manner, the temperature at the base of the calcite–chlorite zone during its formation can be estimated from the fluid-inclusion data. The appearance of epidote in samples from a depth of 616–622 m marks the lower limit of this zone in well A. Fluid inclusions in anhydrite from this depth have homogenization temperatures averaging 282°C.

In contrast, the fluids initially present in the deltaic deposits could not have been the source of the anhydrite and associated calcite cement found in the sandstones. This conclusion is based on the differences in depositional environments between the evaporite and deltaic deposits. However, the fluids in the overlying lacustrine rocks would have been enriched in both sulfate and bicarbonate. Because anhydrite and calcite display retrograde solubilities, heating of downward moving sulfate and carbonate ions would have resulted in the deposition of calcite

and anhydrite in the sandstones immediately underlying the lacustrine deposits. With time, continued diffusion of sulfate and carbonate would have led to a progressive thickening of the sandstones cemented by anhydrite and calcite. The fluid-inclusion data and petrographic relationships discussed below suggest that this cementation has been very effective in reducing the permeabilities and porosities of these rocks.

Fluid-inclusion data suggest that some of the anhydrite contained within the lacustrine deposits was also precipitated directly into the existing pore space. Primary fluid inclusions in anhydrite from a depth of 168–177 m indicate that anhydrite formed at temperatures of 125°C. Because the measured homogenization temperatures are much higher than those required for the dehydration of gypsum to anhydrite (42°C in pure water, Deer *et al.*, 1966), this anhydrite could not represent replacement of original gypsum.

The fluid inclusions contained within anhydrite can be divided into three groups on the basis of their homogenization and ice-melting temperatures (compare Figs 4a and 4b). The first group (group 1) consists of low-temperature, high-salinity inclusions. These inclusions are primary in origin and occur immediately beneath the unconsolidated lacustrine sediments at a depth of 168–177 m. The fluid-inclusion data from this group suggest that the anhydrite was formed by fluids that underwent surface evaporation and migrated downward due to their high density (1.1 g cm^{-3}).

A second group of inclusions is represented by samples from depths between 177 and 378 m (group 2). These inclusions occur in the sandstones cemented by anhydrite and carbonate and have intermediate homogenization and ice-melting temperatures. Inclusions from depths between 460 and 622 m (group 3) have higher homogenization temperatures and slightly lower ice-melting temperatures (higher salinities) than those of group 2. The salinity–depth relationships between groups 2 and 3 are thus consistent with the existence of vertical gradients in the salinity of the brines as proposed by Helgeson (1968).

The homogenization temperatures of the fluid inclusions in anhydrite (refer to Fig. 4a) record generally similar temperature profiles in both wells. These profiles are characterized by high gradients through the upper 323 m in well A and 341 m in well B. Using the average homogenization temperature of 247°C for samples from a depth of 332–341 m in well B and assuming a mean annual air temperature of 22.5°C (Imperial Irrigation District, 1982), the calculated average gradient to this depth is 0.66°C m^{-1}. Younker *et al.* (1982) have shown that such high gradients would be expected where heat transfer is by conduction through rocks of low permeability. We conclude from the calculated gradients and the mineralogic relationships that the thermal cap in these wells extends to the base of the sandstones cemented by anhydrite and calcite. In contrast, homogenization temperatures of inclusions in well A between 460 and 622 m are nearly constant with depth, yielding a low thermal gradient. These data imply that heat is transferred by convection (Younker *et al.*, 1982).

The conclusion that the overall permeabilities within the lacustrine deposits and sandstones cemented by anhydrite and calcite are low cannot be tested directly. However, several observations suggest that this is indeed the case. These observations include: (1) interlocking anhydrite and calcite grains with no visible pore space in the lacustrine sequence; (2) the extensive development of anhydrite and calcite cement in shallow sandstones which typically have initial porosities ranging from 5 to 15% (S. D. McDowell, 1987, written comments); (3) the salinity–temperature relationships of inclusions from the sandstones cemented by anhydrite and calcite. Figures 4a and 4b show that there is a large range in the ice-melting temperatures (salinities) of the fluid-inclusion brines from individual samples, but little temperature range among the same inclusions. Thus, some circulation of brines of varying salinities occurred during and after deposition of the anhydrite cement. However, the volumes and flow rates of these

fluids must have been relatively low because the homogenization temperatures record only a single thermal profile.

A predictable consequence of the downward thickening of the thermal cap is a decrease in rock temperatures with time. The extent of this cooling can be estimated from the differences in the fluid-inclusion homogenization temperatures recorded by the anhydrite cement and by the sphalerite and quartz that was subsequently deposited. For example, the lowest homogenization temperatures in sphalerite from a depth of 305–314 m provide an upper limit of the ambient temperatures during its deposition. These temperatures average 181°C, while the maximum temperatures recorded by anhydrite from the same well average 232°C. Thus, the formation of the thermal cap lowered the temperatures by at least 50°C.

The replacement of detrital plagioclase by potassium feldspar in the shallow deltaic sandstones could not have been produced by the downward percolating fluids or diffusing ions that deposited anhydrite in these rocks. The mineral relationships indicate that the formation of secondary potassium feldspar involved the addition of potassium and removal of sodium from the rocks. Because the K/Na ratio of geothermal waters increases with increasing temperature (Fournier and Truesdell, 1973; Ellis and Mahon, 1977), the formation of potassium feldspar in the shallow deltaic rocks must have resulted from the influx of brines derived from higher-temperature portions of the geothermal system.

The fluids that produced this alteration were also a likely source of zinc, lead and copper. These metals occur in significant concentrations in the modern brines and are common in veins throughout the field (McKibben and Elders, 1985). The textural relationships suggest that the sphalerite cement found in the deltaic sandstones has replaced pre-existing anhydrite cement. This relationship and the absence of pre-existing sulfide mineralization in these rocks (i.e. pyrite or marcasite) implies that the sulfur for sulfide deposition was provided by reduction of either anhydrite or shallow sulfate-rich fluids. Since sulfate-reducing bacteria are not known to function at these temperatures, the most likely reductant of sulfate in the deltaic rocks is reduced carbon. Although reduced carbon is not abundant in these sandstones, it is common in the shallow rocks of the geothermal system (McKibben and Elders, 1985). Thus, the sulfate could have been reduced by hydrocarbons from organic debris and carried in solution by the upwelling brines. Hydrocarbons are present in fluid inclusions contained in sphalerite and vein quartz from well B and have also been found in production fluids from the Cerro Prieto and Niland fields in the Salton Trough (Nehring and Truesdell, 1978; D. Michels, personal communication, 1984). The precipitation of sphalerite by sulfate reduction is given by the reactions (Anderson, 1983):

$$SO_4^{2-} + CH_4 + Zn^{2+} = \text{sphalerite} + CO_2 + 2H_2O \quad (1)$$

and

$$\text{anhydrite} + CH_4 + Zn^{2+} = \text{sphalerite} + Ca^{2+} + CO_2 + 2H_2O. \quad (2)$$

The occurrence of significant sphalerite cement within the lower part of the thermal cap implies that matrix permeabilities were relatively high during its deposition. Although the permeabilities that allowed the influx of metal-bearing fluids into these rocks may have developed initially in response to seismic activity, they could have been subsequently enhanced by the dissolution of anhydrite and calcite as the brines migrated laterally away from the upflow zones and cooled. This cooling would also have resulted in deposition of the quartz overgrowths found in the rocks containing secondary potassium feldspar and sphalerite.

In contrast, the formation of veins implies lower matrix permeabilities and fracture-dominated fluid flow (Elders, 1979). These relationships suggest that the quartz veins occurring in the shallow parts of well B postdate the sphalerite cement and mark the development of fracture

permeability in this well. Unlike the veins occurring in other parts of the geothermal system (see for example McKibben and Elders, 1985), the shallow veins in well B contain barite. Textural relationships indicate that the barite was precipitated and resorbed prior to the deposition of the base-metal sulfides that occur in the veins. Similar paragenetic relationships have been described by Barnes (1983) from Mississippi Valley lead–zinc deposits. Because of the low solubility of barite at moderate temperatures (100–200°C), Barnes (1983) concluded that the deposition of barite would most likely occur where barium-bearing solutions encountered a sulfate-rich groundwater or where oxidation of sulfide to sulfate in solution can occur. As discussed above, sulphate-bearing pore fluids must have been present in the sandstones in the upper part of the deltaic section and could have mixed with the rising vein fluids where barite was deposited. Later, these fluids would have been purged from the veins as upward flow continued, causing dissolution of early barite and deposition of sulfides, hematite and additional quartz from further cooling.

SUMMARY AND CONCLUSIONS

Fluid-inclusion data and petrographic studies have been used to reconstruct the evolution of the rocks in the shallow portions of two wells drilled in the southern part of the Salton Sea geothermal system. The rocks encountered in these wells can be divided into an upper sequence of lacustrine claystone and evaporite deposits with low initial permeabilities (Randall, 1974) and an underlying deltaic sequence of sandstones with high initial permeabilities, siltstones, and shales. The base of the lacustrine deposits ranges from depths of 241 to 277 m in the two wells studied.

The initial heating of these rocks resulted in the formation of anhydrite after gypsum and the formation of secondary chlorite and illite from reactions involving detrital and secondary phyllosilicates. Anhydrite and calcite were also deposited directly from the pore fluids as a cement in the underlying deltaic sandstones. Cementation of the sandstones progressed downward, reducing their permeabilities. Fluid-inclusion homogenization temperatures in anhydrite increase systematically with depth through the sandstones cemented by anhydrite and calcite, but display little variation within individual depth intervals. In contrast, large variations in the salinities of these fluid inclusions demonstrate that some mixing of downward-percolating brines and geothermal fluid took place during formation of the inclusions. However, the velocities of the descending waters were generally not high enough to disturb the thermal gradient.

The fluid-inclusion data yield an average thermal gradient of $0.66°C\ m^{-1}$ between the surface and a depth of 341 m. We infer from this high thermal gradient that heat is being transferred through the lacustrine deposits and sandstones cemented by anhydrite and calcite by conduction and that these rocks act as a low permeability thermal cap over the reservoir in the two wells studied. Homogenization temperatures in anhydrite between 460 and 622 m range from 272 to 288°C and are nearly constant with depth, suggesting that heat is transferred primarily by convection in this zone.

The influx of brines from higher-temperature portions of the geothermal system occurred episodically during development of the thermal cap. Movement of these brines through the lower portions of the thermal cap resulted in the deposition of potassium feldspar, quartz and sphalerite cement. The abundance of pore-filling sphalerite within the deltaic sandstones suggests that permeabilities were relatively high during its deposition. An increase in permeability could have resulted from the dissolution of calcite and anhydrite cement by the cooling brines.

The transition from matrix to fracture permeability in the shallow parts of one of the wells is

reflected in the formation of quartz veins. These veins consist dominantly of quartz with minor barite, hematite, chlorite and base-metal sulfides.

Acknowledgements—We would like to thank R. Dondanville and G. Suemnicht of UNOCAL for providing the samples and making this study possible. T. J. Reynolds shared his knowledge of fluid inclusions with us and made many helpful suggestions during the course of the project. M. Sommer performed the gas analyses of the inclusions. B. Miller prepared the polished plates for the fluid-inclusion studies and performed some of the heating measurements. The X-ray diffraction patterns were prepared by L. McPherson. J. Hulen assisted in the interpretation of the X-ray data. J. Ballantyne, R. Fournier, J. Hulen, S. D. McDowell, L. J. P. Muffler, T. J. Reynolds, E. Roedder and P. M. Wright critically reviewed earlier versions of this manuscript and made many helpful suggestions. P. Daubner drafted the illustrations and K. Ruth typed the manuscript. Their assistance is greatly appreciated.

Funding for this project was provided by the Department of Energy under Contract Number DE-AC03-84SF12196.

REFERENCES

Anderson, G. M. (1983) Some geochemical aspects of sulfide precipitation in carbonate rocks. In: *International Conference on Mississippi Valley Type Lead–Zinc Deposits. Proc. Vol.* (Edited by Kisvarsanyi, G., Grant, S. K., Pratt, W. P. and Koenig, J. W.), pp. 61–76. University of Missouri-Rolla.

Andes, J. P., Jr. and McKibben, M. A. (1987) Thermal and chemical history of mineralized fractures in cores from the Salton Sea scientific drilling project (abstract). *Eos Trans. AGU.* **68**, 439.

Barnes, H. L. (1983) Ore-depositing reactions in Mississippi Valley-type deposits. In: *International Conference on Mississippi Valley Type Lead–Zinc Deposits. Proc. Vol.* (Edited by Kisvarsanyi, G., Grant, S. K., Pratt, W. P. and Koenig, J. W.), pp. 77–85. University of Missouri-Rolla.

Bodnar, R. J. and Bethke, P. M. (1984) Systematics of stretching of fluid inclusions I: fluorite and sphalerite at one atmosphere confining pressure. *Econ. Geol.* **79**, 141–161.

Deer, W. A., Howie, R. A. and Zussman, J. (1966) *An Introduction to the Rock-Forming Minerals.* John Wiley, New York.

Elders, W. A. (1979) The geological background of the geothermal fields of the Salton Trough. In: *Geology and Geothermics of the Salton Trough* (Edited by Elders, W. A.), pp. 1-19. Campus Museum Contribution, University of California, Riverside 5.

Elders, W. A. and Cohen L. H. (1983) The Salton Sea geothermal field, California, as a near-field natural analog of a radioactive waste repository in salt. Battelle Memorial Inst. Office of Nuclear Waste Isolation, BMI/ONWI-513.

Ellis, A. J. and Mahon, W. A. J. (1977) Natural hydrothermal systems and experimental hot water/rock interactions, Part 2. *Geochim. cosmochim. Acta* **31**, 519–538.

Fournier, R. O. and Truesdell, A. H. (1973) An empirical Na-K-Ca geothermometer for natural waters. *Geochim. cosmochim. Acta* **37**, 1255–1275.

Freckman, J. T. (1978) Fluid inclusion and oxygen isotope geothermometry of rock samples from Sinclair #4 and Elmore #1 boreholes, Salton Sea geothermal field, Imperial Valley, California, U.S.A. M.Sc. Thesis. University of California, Riverside.

Haas, J. L. Jr. (1971) The effect of salinity on the maximum thermal gradient of a hydrothermal system at hydrostatic pressure. *Econ. Geol.* **66**, 940–946.

Huang, C. I. (1977) Fluid inclusion study of well cuttings from Magmamax #2 drillhole, Salton Sea geothermal area, California (abstract). *Econ. Geol.* **72**, 730.

Helgeson, H. C. (1968) Geological and thermodynamic characteristics of the Salton Sea geothermal system. *Am. J. Sci.* **266**, 129–166.

Imperial Irrigation District, Imperial Valley Annual Weather Summary (1982) Monthly high, low and mean temperatures and rainfall, 1914–1982. Community and Special Services, Imperial Irrigation District, El Centro, CA.

Larson, L. T., Miller, J. D., Nadeau, J. E. and Roedder, E. (1973) Two sources of error in low temperature inclusion homogenization determination and corrections on published temperatures for the East Tennessee and Laisvall deposits. *Econ. Geol.* **68**, 113–116.

Lawler, J. P. and Crawford, M. L. (1983) Stretching of fluid inclusions resulting from a low-temperature microthermometric technique. *Econ. Geol.* **78**, 527–529.

McDowell, S. D. and Elders, W. A. (1979) Geothermal metamorphism of sandstone in the Salton Sea geothermal system. In: *Geology and Geothermics of the Salton Trough* (Edited by Elders, W. A.), pp. 70–76. Campus Museum Contribution, University of California, Riverside 5.

McDowell, S. D. and Elders, W. A. (1980) Authigenic layer silicate minerals in borehole Elmore 1, Salton Sea geothermal field, California, U.S.A. *Contrib. Mineral. Petrol.* **74**, 293–310.

McDowell, S. D. and Elders, W. A. (1983) Allogenic layer silicate minerals in borehole Elmore #1, Salton Sea geothermal systems. *Am. Mineral.* **68**, 1146–1159.

McDowell, S. D. and Paces, J. B. (1985) Carbonate alteration minerals in the Salton Sea geothermal system, California, U.S.A. *Mineral. Mag.* **49**, 469–479.

McKibben, M. A. and Elders, W. A. (1985) Fe–Zn–Cu–Pb mineralization in the Salton Sea geothermal system, Imperial Valley, California. *Econ. Geol.* **80**, 539–559.

Muffler, L. J. P. and Doe, B. R. (1968) Composition and mean age of detritus of the Colorado River delta in the Salton Trough, southeastern California. *J. Sed. Petrol.* **38**, 384–399.

Muffler, L. J. P. and White, D. E. (1969) Active metamorphism of upper Cenozoic sediments in the Salton Sea geothermal field and the Salton Trough, southeastern California. *Geol. Soc. Am. Bull.* **80**, 157–182.

Nehring, N. L. and Truesdell, A. H. (1978) Hydrocarbon gases in some volcanic and geothermal systems. *Geothermal Res. Counc. Trans.* **2**, 483–486.

Potter, R. W. II, Clynne, M. A. and Brown, D. L. (1978) Freezing point depression of aqueous sodium chloride solutions. *Econ. Geol.* **73**, 284–285.

Randall, W. (1974) An analysis of the subsurface structure and stratigraphy of the Salton Sea geothermal anomaly, Imperial Valley, California. Ph.D. Thesis. University of California, Riverside.

Roedder, E. (1979) Fluid inclusions as samples of ore fluids. In: *Geochemistry of Hydrothermal Ore Deposits* (Edited by Barnes, H. L.), pp. 684–736. John Wiley, New York.

Roedder, E. and Howard, K. W. (1987) Fluid inclusions in SSSDP core: Preliminary results (abstract). *Eos Trans. AGU* **68**, 439.

Skinner, B. J., White, D. E., Rose, H. J. and Mays, R. E. (1967) Sulfides associated with the Salton Sea geothermal brine. *Econ. Geol.* **62**, 316–330.

Sommer, M. A., II (1974) Analysis and interpretation of the gases released from various sites in rocks and minerals. Ph.D. Thesis, University of Tulsa, Oklahoma.

Sommer, M. A., II, Yanover, R. N., Bourcier, W. L. and Gibson, E. K. (1985) Determination of H_2O and CO_2 concentrations in fluid inclusions in minerals using laser decrepitation and capacitance manometer analysis. *Anal. Chem.* **57**, 449–453.

Srodon, J. and Eberl, D. D. (1984) Illite. In: *Micas* (Edited by Bailey, S. W.), pp. 495–544. Reviews in Mineralogy, Volume 13, Mineralogical Society of America.

Younker, L. W., Kasameyer, P. W. and Tewhey, J. D. (1982) Geological, geophysical and thermal characteristics of the Salton Sea geothermal field, California. *J. Volcano. Geotherm. Res.* **12**, 221–258.